#### **Physical Chemistry**

Nishant Bhardwaj, Pooja Sharma and Vineet Kumar\*

# Oryza sativa plant extract in 15% hydrochloric acid as a green corrosion inhibitor on the surface of stainless steel 410

https://doi.org/10.1515/tsd-2021-2355 Received February 26, 2021; accepted August 23, 2021

Abstract: Fifteen percent hydrochloric acid (HCl) solutions are used for some cleaning processes in the petroleum industry. The use of such a corrosive medium is mainly responsible for the corrosion of the stainless steel (SS-410) vessels and pipings. In this study, the corrosion inhibiting properties of Oryza sativa plant extract (OSPE) from agricultural residues are investigated on SS-410 steel surfaces in a 15% HCl medium. Gravimetric analysis showed a maximum corrosion inhibition of 91.92% with 4 g/L OSPE in 15% HCl solution. Scanning electron microscopy (SEM), atomic force microscopy (AFM), and X-ray diffraction studies confirmed the adsorption of OSPE on the SS-410 surface. The adsorption of OSPE on SS-410 followed the Langmuir adsorption isotherm, indicating the formation of a monolayer on the SS-410 surface. The theoretical study confirmed that the anticorrosive effect could be mainly related to the phytochemical 9,12,15-octadecatrienoic acid 2,3-dihydroxypropyl ester. Consequently, the OSPE containing this phytochemical shows an anticorrosive behavior on the SS-410 surface in an acidic 15% HCl solution.

**Keywords:** atomic force microscopy (AFM); electrochemical impedance spectroscopy; green corrosion inhibitor; Langmuir adsorption isotherm; *Oryza sativa plant extract* (OSPE); potentiodynamic polarization (PDP).

E-mail: vineetkumar22@gmail.com.

https://orcid.org/0000-0002-8772-679X

Nishant Bhardwaj, Department of Chemistry, Lovely Professional University, Phagwara 144411, India,

E-mail: nishu.bhardwaj57@gmail.com

**Pooja Sharma**, Department of Biotechnology, Lovely Professional University, Phagwara 144411, India,

E-mail: sharmapooja566@ymail.com

#### 1 Introduction

Every year around 75,000 billion USD are lost due to corrosion. It accounts for 3.4% of world's GDP loss. In India, corrosion causes loss of 1670 billion USD which is equivalent to 4.2% of the total GDP [1]. Metal corrosion is one of the biggest problems faced by many industries. Efforts are continuously being made to find suitable solutions to this major issue [2–7]. Fe–Cr–C alloys have been specially developed for components requiring higher mechanical strength and high to medium corrosion resistance. The 400 series stainless steel is one of the martensitic steels widely used in the petroleum industry, especially in oil production and refining for turbine components, fasteners and machine parts [8].

Various industrial processes namely acid pickling, acid cleaning, and descaling, oil well acidization utilizes mineral acids. HCl and sulfuric acid ( $\rm H_2SO_4$ ) are commonly used mineral acids [9]. Use of  $\rm H_2SO_4$  leads to the formation of insoluble products. Therefore, petroleum industries mostly use 15% HCl for descaling purpose as no insoluble products are left after the treatment. In addition, the process is commercially feasible and cost-effective. The use of HCl also has some limitations as it affects the metallic surface of the machine parts during the cleaning process, leading to corrosion [10].

The destruction of metal components can be avoided by using corrosion inhibitors [11, 12]. Most inhibitors that are used in an acid-aggressive environment and prevent the dissolution of the metal by acid attack contain organic compounds as the main components. These compounds contain nitrogen, oxygen and/or sulfur atoms, heterocyclic compounds and  $\pi$ -electrons. The inhibitors for acidic environments are absorbed on the surface of stainless steel by physisorption or chemisorption or both and thus prevent corrosion. Among the different types of corrosion inhibitors, so-called green corrosion inhibitors are preferred as they are environmentally friendly and cost-effective. Green corrosion inhibitors based on plant extracts are of particular interest. The use of plant waste in the extraction of the plant extracts

<sup>\*</sup>Corresponding author: Vineet Kumar, Department of Biotechnology, Lovely Professional University, Phagwara 144411, India,

is particularly noteworthy, as it additionally reduces the accumulation of waste in the environment and helps farmers to earn money from waste [13–16].

*Oryza sativa* is a grass diverse genus with 25–30 species of deciduous flowering plants in the family Poaceae and is also known as Chawal or Kanak in India. The image of the *O. sativa* plant is shown in Figure 1 [17]. The *O. sativa* residues contain various types of phytochemicals as mentioned in Figure 1. After harvesting the seeds most of the vegetative residues are unutilized and discarded to end up as waste in the environment. Most of these residues are burned in India as there are no strategies to fully recycle them, thus the residues contribute to environmental pollution.

The aim of this work is to explore the adsorptive and corrosion inhibiting properties of *O. sativa* plant extract (OSPE) in order to obtain statements on the use of OSPE as a corrosion inhibitor on SS-410 surfaces in 15% HCl. This work focuses on the efficient use of *O. sativa* plant residues, which have so far been treated as waste.

### 2 Experimental

## 2.1 Oryza sativa plant extract and working electrode preparation

For the preparation of the working electrode, stainless steel samples SS-410 with a diameter of 10 mm were immersed in epoxy resin. The elemental composition of the stainless steel used was Fe (87.2%), Cr

(11.14%), Mn (0.82%), Cu (0.43%), C (0.134%), P (0.02%), and Si (0.005%). The surface of the working electrode was abraded with 100, 320, 600, 800, 1000, and 1200 grit emery paper.

*O. sativa* plant waste was collected from agricultural land near Jalandhar, Punjab, India and its identification was done by Botanical Survey of India, Dehradun. The plants were dried in the sun shade for two days and ground into powder. Hundred grams of the powder was extracted with 450 ml methanol at 75 °C for 72 h. The extracted solution was filtered. The pH of the aqueous solution was nine.

The filtrate was evaporated using a Soxhlet evaporator. The resulting liquid extract was then completely dried in a vacuum desiccator to obtain OSPE. The OSPE was then dissolved in 15% HCl. This solution is used as the corrosive medium in the following. Corrosive medium solutions with different concentrations of OSPE (1 g/L, 2 g/L, 3 g/L, and 4 g/L) were prepared.

#### 2.2 Weight loss measurement

To determine the weight loss, tests were carried out with (1–4) g/L OSPE in 15% HCl medium at room temperature for 24 h [18]. The SS-410 samples measuring 5 cm  $\times$  5 cm  $\times$  0.3 cm were weighed and immersed in the test solutions both in the presence and absence of OSPE for 24 h. Then, the SS-410 samples were removed from the test solution, rinsed with acetone, dried under nitrogen flow, and weighed.

#### 2.3 Electrochemical impedance spectroscopy

Auto lab electrochemical work station (Metrohm) with three-electrode electrochemical cell was used for the measurements of the electrochemical impedance and the Tafel polarization. The obtained Tafel polarization curves were recorded between –200 mV and +200 mV versus Ag/AgCl (3 M KCl) with a scanning rate of 0.1 mV/s. The

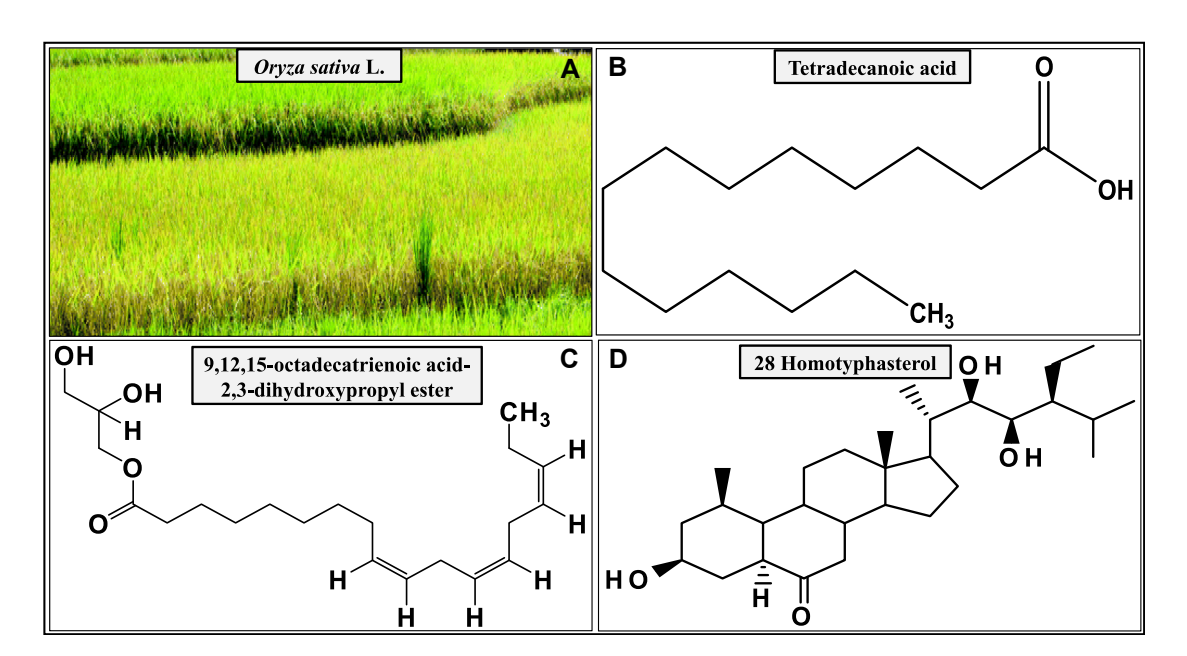


Figure 1: (A) Image of *Oryza sativa*. Molecular structure of phytochemicals present in *O. sativa*: (B) tetradecanoic acid, (C) 9, 12, 15-octadecatrienoic acid- 2, 3-dihydroxypropyl ester, (D) 28-homotyphasterol.

electrochemical measurements were conducted at 10 mV amplitude in a frequency range from 100 kHz to 0.01 Hz. The obtained data were calculated by using CHI 760C electrochemical work station software.

#### 2.4 Fourier Transform Infra-Red (FTIR) spectroscopic study

The Fourier Transform Infra-Red (FTIR) spectra were recorded between (500-4000) cm<sup>-1</sup> to identify the functional groups present in the phytochemicals of the OSPE. The FTIR 8400S spectrophotometer (Shimadzu) was used for FTIR measurements. The FTIR spectra of OSPE were also recorded at different conditions prior to immersion of SS-410 in 4 g/L OSPE in 15% HCl.

#### 2.5 Ultraviolet-visible spectroscopic study

The preliminary anticorrosion activity of OSPE prepared in 15% HCl solution were investigated using UV-vis 1800 spectrophotometer (Shimadzu). The UV-vis analysis was performed using two set of experiments. In both set of condition, SS-410 was immersed in HCl solution. In the first set of conditions, the UV-vis spectrum of 15% HCl solution containing 4 g/L OSPE was recorded. In the second set of condition, the spectrum was recorded for 15% HCl solution in absence of OSPE.

#### 2.6 Surface investigation

- 2.6.1 Atomic force microscopic study: The INTEGRA atomic force microscopy (AFM) model (NT-MDT) was used to study the stainless steel surface SS-410. For the AFM study, the SS-410 surface was cleaned with ultrapure water and then with acetone. Samples of the abraded SS-410, the SS-410 immersed in corrosive media and the SS-410 immersed in 15% HCl solution with 4 g/L OSPE were characterized by AFM.
- **2.6.2 Scanning electron microscopic analysis:** The scanning electron microscope (SEM, JEOL) was used for taking the surface micrograph of SS-410. SEM images were captured for polished SS-410 and SS-410 samples immersed in corrosive media in the absence and presence of 4 g/L OSPE.
- 2.6.3 X-ray diffraction (XRD) analysis: The PHI 5000 Versa Probe III model (Physical Electronics, Inc.) was used for the XRD study. Prior to measurement, the SS-410 stainless steel samples were immersed in a 15% HCl solution with and without 4 g/L OSPE, then the SS-410 samples were dried and measured using the above instrument. The corrosion inhibitor adsorption process on the SS-410 surface was explained on the basis of the XRD study.

#### 2.7 Theoretical studies

The computer programme Hyperchem (8.0) was used for the theoretical studies of the corrosion protection effect of the phytochemicals contained in OSPE. The experiments were analyzed using density functional theory (DFT). The energies of the frontier molecular orbitals were used as the main parameters for this evaluation.

#### 3 Results and discussion

#### 3.1 Weight loss measurement

Corrosion inhibition efficiency (IE) of OSPE was calculated for the surface of SS-410 in the presence of 15% HCl medium. The rate of SS-410 corrosion in corrosive media containing different concentration of OSPE was calculated using Equation (1):

$$C_R = \frac{K \times W}{A \times t \times \rho} \tag{1}$$

where,  $C_R$  is the corrosion rate (mm year<sup>-1</sup>), W is the weight loss of stainless steel (SS-410), K the corrosion constant  $(8.76 \times 10^4)$ , A is the exposed area in cm<sup>2</sup>, t is the immersion time (h) of SS-410,  $\rho$  is the density (7.86 g cm<sup>-3</sup>) of the steel according to the ASTM G 31-72 standard [19].

The value of corrosion IE and surface coverage ( $\theta$ ) of OSPE was calculated by Equations (2) and (3):

$$IE = \frac{C_R^0 - C_R^i}{C_R^0} \times 100 \tag{2}$$

$$\theta = \frac{C_R^0 - C_R^i}{C_R^0} \tag{3}$$

where, the corrosion rate of SS-410 immersed in the corrosive media (15% HCl) and the corrosive media containing OSPE solution was mentioned by  $C_R^0$  and  $C_R^i$ , respectively. As the concentration of OSPE in 15% HCl increases, the value of corrosion rate decreases thus leading to increase in IE. The decrease in the value of corrosion rate was due to adsorption of OSPE phytochemicals on the surface of SS-410. A maximum of 91.92% IE was recorded for the aggressive medium containing 4 g/L OSPE. The values of the main parameters are shown in Table 1.

#### 3.2 Adsorption isotherm studies

Adsorption isotherms are generally used to obtain information on the nature of the interaction of molecules on the substrate surface (here: stainless steel SS-410) by adsorption. In this work, the experimental data were fitted using the adsorption isotherms of Langmuir, Temkin, Frumkin, Freundlich, Flory-Huggins, and El-Awady (Equations (4)-(9):

Langmuir isotherm 
$$\frac{C_{\text{inh}}}{\theta} = \frac{1}{K_{\text{ads}}} + C$$
 (4)

El-Awady isotherm 
$$\ln\left(\frac{\theta}{1-\theta}\right) = \ln K_{\text{ads}} + y \ln C_{\text{inh}}$$
 (5)

**Table 1:** Weight loss parameters for different concentrations of hydrochloric acid (HCl) with *Oryza sativa* plant extract (OSPE) after 24 h at 298 K.

Concentration	Corrosion rate C <sub>R</sub> /mmy <sup>-1</sup>	Inhibition efficiency IE/%	Surface coverage $ heta$	С/Ө	Equilibrium adsorption constant $ m K_{ads}/L~g^{-1}$
15% HCl	39.01				
15% HCl + 1 g/L OSPE	13.181	66.21	0.6621	1.51	1.96
15% HCl + 2 g/L OSPE	9.630	75.31	0.7531	2.65	1.53
15% HCl + 3 g/L OSPE	6.120	84.31	0.8431	3.55	1.81
15% HCl + 4 g/L OSPE	3.152	91.92	0.9192	4.35	2.85

Flory-Huggins isotherm 
$$\ln\left(\frac{\theta}{C_{\text{inh}}}\right)$$
  
=  $\ln K_{\text{ads}} + x \ln(1 - \theta)$  (6)

Freundlich isotherm  $\ln(\theta) = \ln K_{\text{ads}} + z \ln C_{\text{inh}}$  (7)

Frumkin isotherm 
$$\ln \left[ \left( \frac{\theta}{1 - \theta} \right) * \frac{1}{C_{\text{inh}}} \right] = -\ln K_{\text{ads}} + 2 d\theta$$
 (8)

Temkin isotherm 
$$\theta = -\frac{1}{2a} \ln K_{\text{ads}} - \frac{1}{2a} \ln C_{\text{inh}}$$
 (9)

The value of regression coefficient  $(R^2)$  follows the order: Langmuir isotherm > Freundlich isotherm > Temkin isotherm > El-Awady isotherm > Flory-Huggins isotherm > Frumkin isotherm, as shown in Figure 2A-F. It can be concluded that the adsorption of OSPE on SS-410 best follows the Langmuir adsorption isotherm, since in this case the value of  $R^2$  is closest to one compared to those of the other isotherms. The Langmuir isotherm could indicate that one or more inhibitor units occupy multiple adsorption sites. It also seems to indicate that interactions occur between the metal surface and the OSPE species adsorbed on the SS-410 surface or that a change in the heat of adsorption (enthalpy) occurs with increasing surface coverage [20]. Therefore, Langmuir adsorption isotherm was used for explaining the adsorption behavior of OSPE on the SS-410 surface. The concentration of OSPE used and the value of OSPE surface coverage provided to SS-410 were the main parameter of this study. The function of  $C/\theta$  and C was recorded and plotted in Figure 2A.  $K_{\rm ads}$  is used for equilibrium adsorption constant (Table 1).

#### 3.3 Electrochemical study

#### 3.3.1 Potentiodynamic polarization

The working electrode of SS-410 was immersed in 15% HCl solutions with fixed OSPE concentrations of 1 g/L, 2 g/L,

3 g/L, and 4 g/L. As the results in Table 2 show, the current densities decrease with the increase of OSPE concentration from 1 g/L to 4 g/L.

The value of IE was calculated using Equation (10) [21].

$$IE = \frac{I_{\text{corr}}^0 - I_{\text{corr}}^i}{I_{\text{corr}}^0} \times 100 \tag{10}$$

where  $I_{\text{corr}}^0$  and  $I_{\text{corr}}^i$  were used for corrosion current density of 15% HCl solution and OSPE inhibitor solution.

The polarization curve is shown in Figure 3. The potential scans were performed in the positive direction. The observed behavior indicates that the more inhibitor present in the solution, the better the protection of SS-410. In addition, the results showed that the rate at which OSPE adsorbs on SS-410 depends on the OSPE concentration. The higher the OSPE concentration in the corrosive media, the lower the corrosion current density value, which means an increase in IE.

It has already been reported that the inhibition is anodic when the maximum shift of the corrosion potential  $(E_{\rm corr})$  in the acidic solution is greater than 85 mV [22, 23]. It can be concluded that OSPE follows an anodic inhibition mechanism. The OSPE inhibitor is adsorbed on the SS-410 surface, forming a protective film or barrier that causes a large anodic shift, thereby reducing the corrosion rate. In addition, the potential shift forces the metallic surface into the passivation region. With 4 g/L OSPE in 15% HCl solution, a maximum IE of 76.44% was achieved.

#### 3.3.2 Electrochemical impedance spectroscopy

The working electrode of SS-410 was immersed in 15% HCl solutions with different concentration of OSPE. Figure 4 shows the Nyquist plots. Each of the curves shown contains a semicircle representing a constant time, which is due to the charge transfer resistance. As the OSPE concentration increases from 1 g/L to 4 g/L, the diameter of the circle increases. However, this also means an increase in IE, which was calculated using Equation (11) [8].

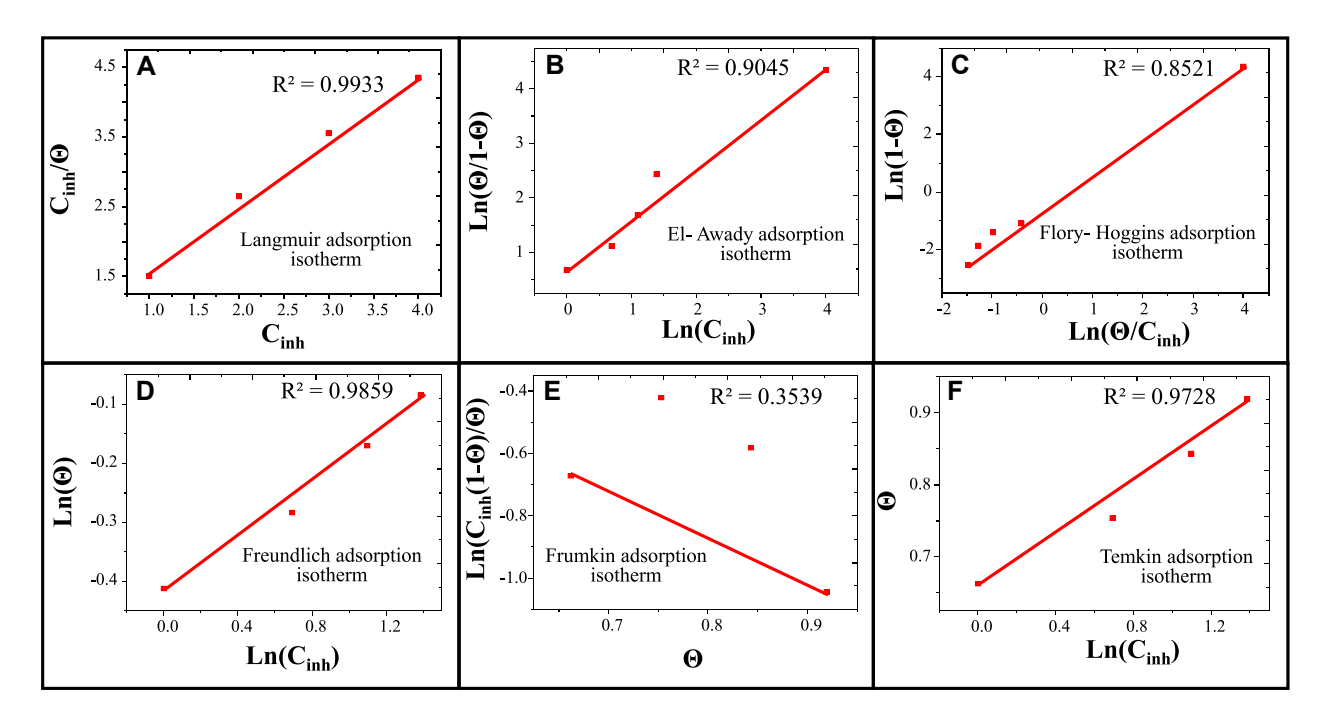


**Figure 2:** Adsorption isotherms (A) Langmuir adsorption isotherm, (B) El-Awady adsorption isotherm, (C) Flory-Higgins adsorption isotherm, (D) Freundlich adsorption isotherm, (E) Frumkin adsorption isotherm, and (F) Temkin adsorption isotherm; the experimental data follow Langmuir adsorption isotherm as  $R^2$  is near to one, based on weight loss measurements of the OSPE on SS-410 surface 15% hydrochloric acid (HCl) for 24 h.

$$IE = \frac{R_{\rm ct} - R_{\rm ct}^o}{R_{\rm ct}} \times 100$$
 (11)

Here  $R_{\rm ct}$  and  $R_{\rm ct}^o$  denote the charge transfer resistance of the OSPE solutions (1 g L<sup>-1</sup>, 2 g L<sup>-1</sup>, 3 g L<sup>-1</sup>, and 4 g L<sup>-1</sup>) in 15% HCl and of a 15% HCl solution without OSPE, respectively. As can be seen from Table 3, the IE increased with increasing concentration of OSPE in the 15% HCl solution, a maximum IE of 73.00% was obtained for the OSPE concentration of 4 g L<sup>-1</sup> in 15% HCl. From the increasing  $R_{\rm ct}$ 

**Table 2:** Polarization parameters for SS-410 steel in 15% hydrochloric acid (HCl) without *Oryza sativa* plant extract (OSPE) extract and at different concentrations of OSPE extract and 298 K.

Corrosive solution	Corrosion potential E <sub>corr</sub> /mV	Corrosion current density $I_{corr}/A \text{ cm}^{-2}$	Inhibition ef- ficiency IE/%
15% HCl solution	-474.1	0.000054003	_
15% HCl solu-	-352.0	0.000035064	35.07
tion + 1 g/L OSPE			
15% HCl solu-	-352.6	0.000032634	39.57
tion + 2 g/L OSPE			
15% HCl solu-	-350.0	0.000019284	64.29
tion + 3 g/L OSPE			
15% HCl solu-	-358.4	0.000012615	76.64
tion + 4 g/L OSPE			

values (shown in Table 3), a layer formation at the substrate surface can be concluded [24]. It can be assumed that the OSPE is adsorbed on the surface of SS-410, due to the binding of the  $\pi$ -electrons of the aromatic ring or the heteroatoms present in the phytochemicals with the free d-orbital of iron in the SS-410 surface. This process is responsible for the anticorrosive property of OSPE. To

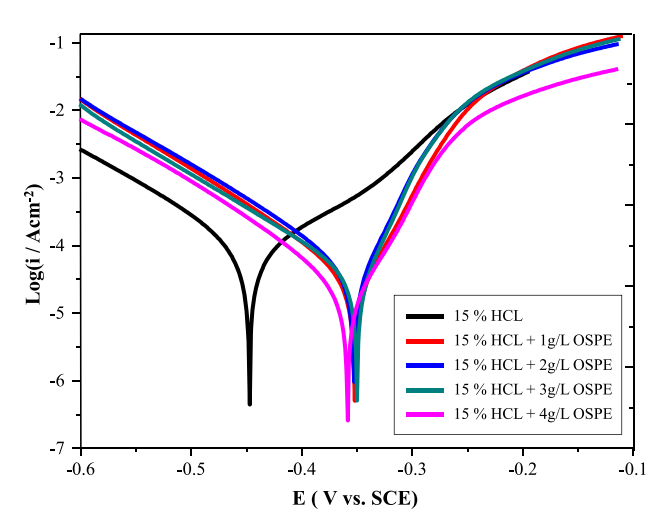


**Figure 3:** Tafel polarization curves for stainless steel (SS) in 15% hydrochloric acid (HCl) solution without and with different concentrations of *Oryza sativa* plant extract (OSPE).

represent the reaction at the interface between electrode and electrolyte, an equivalent circuit was created with Z simpwimp V3.20 (Figure 5). The Bode diagram shown in Figure 6 supports the statement that the OSPE adsorbs to the iron at the surface of SS-410 [25, 26].

It was found that the corrosion rate increases with increasing temperature in HCl solutions without OSPE as well as in HCl solutions with OSPE. Similarly, it was observed that the inhibition effect of the inhibitor decreases with decreasing temperature. The interface between the electrode and the adjacent solution forms a boundary layer known as the double layer capacitance (dlc). It is an important feature of the electrical double layer. At the boundary between the two layers, the charges on the surface of the electrode and the electrolyte are opposite. The dlc values decreased with increasing OSPE concentration. This decrease indicates the adsorption of molecules form the OSPE solution on the surface of SS-410.

The electrochemical impedance spectroscopy (EIS) results agreed with the potentiodynamic polarization (PDP) results. Based on the results, it can be assumed that the active components of the OSPE are involved in the chemical adsorption on the SS-410 surface. The IE decreased with increasing incubation temperature and increased with increasing OSPE concentration. This is due to the fact that OSPE tends to adsorb more on the SS-410 surface at lower temperatures and higher OSPE concentration. The observed difference between the percentage IE

**Table 3:** Electrochemical impedance spectroscopy (EIS) parameters for SS-410 steel in 15% HCl without *Oryza sativa* plant extract (OSPE) extract and at different concentrations of OSPE extract and 298 K.

Corrosive solution	Charge transfer resistance $R_{\rm ct}/\Omega~{ m cm}^{-2}$	Inhibition efficiency IE/%
15% HCl solution	180.21	_
15% HCl solution + 1 g/L OSPE	258.73	30.34
15% HCl solution + 2 g/L OSPE	285.78	36.94
15% HCl solution + 3 g/L OSPE	439.48	58.99
15% HCl solution + 4 g/L OSPE	667.57	73.00

values obtained with EIS and PDP could be due to the different nature of the technique used. PDP measurements provided the real-time kinetics of the electrochemical processes (polarization in a wide potential range with a possible irreversible change due to the measurement process), while EIS data are usually obtained at the OCP (open circuit potential) and provide measurements of the total interfacial resistance at the electrode-electrolyte interface [26, 27].

#### 3.4 FTIR spectroscopic study

The FTIR spectrum presented in Figure 7 indicates the presence of the different functional groups in the OSPE.

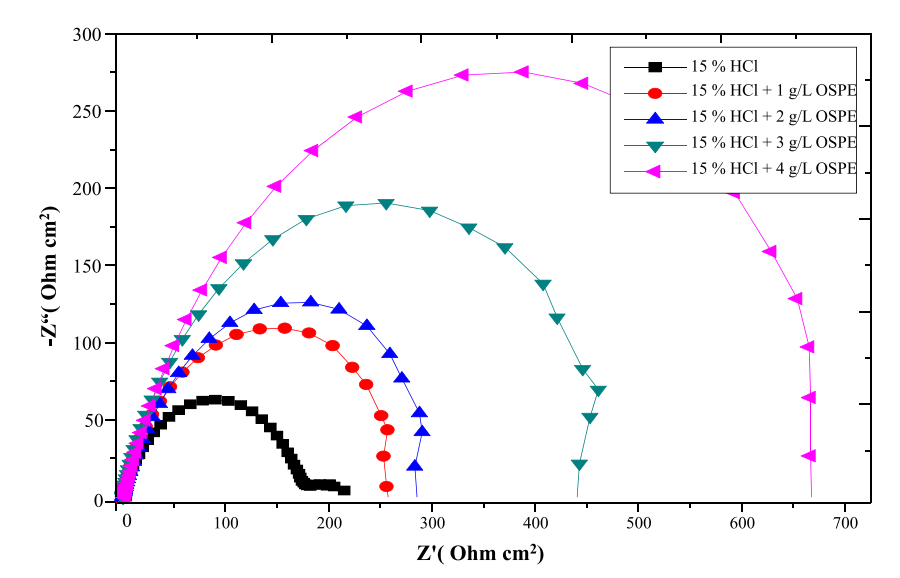


Figure 4: Impedance data of SS-410 in 15% hydrochloric acid (HCI) without and with the different concentrations of OSPE at 298 K.

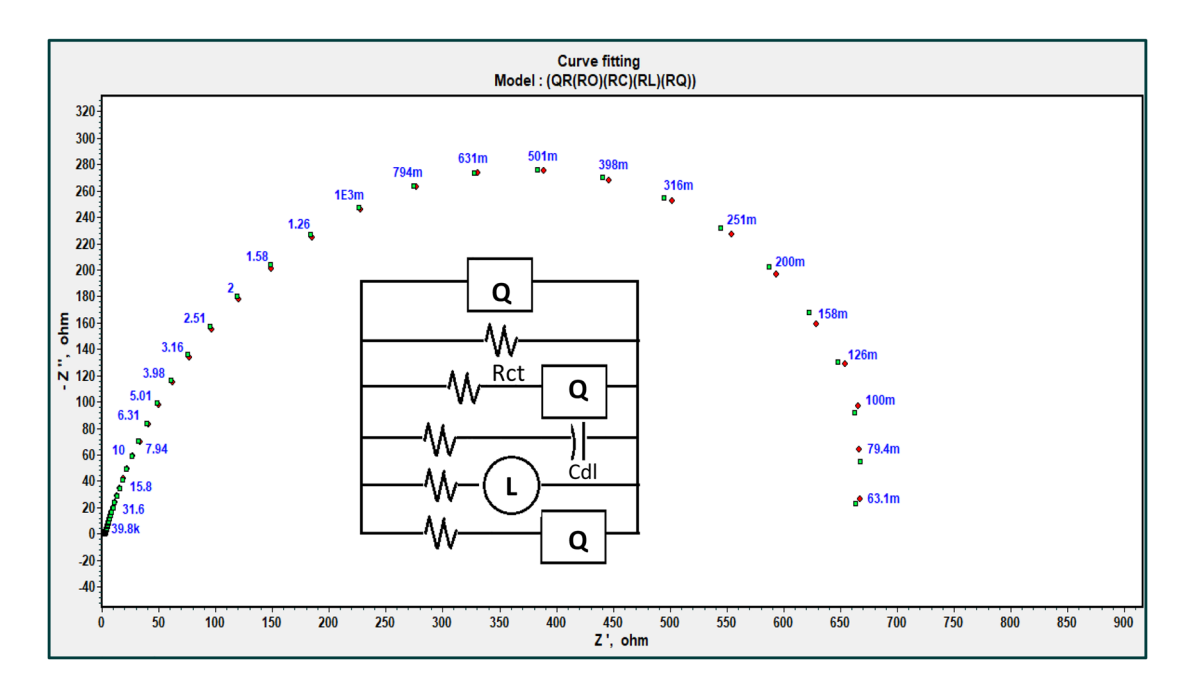


Figure 5: Impedance data curve fitting with equivalent circuit.

The peak at 3327 cm<sup>-1</sup> indicates the presence of the O-H group and the peak at 988 cm<sup>-1</sup> indicates the C=O stretching. The peak at 1429 cm<sup>-1</sup> can be attributed to the vibrations of the aromatic ring. The corrosion-inhibiting property of OSPE can be attributed to the heteroatoms present in the extract [26, 27].

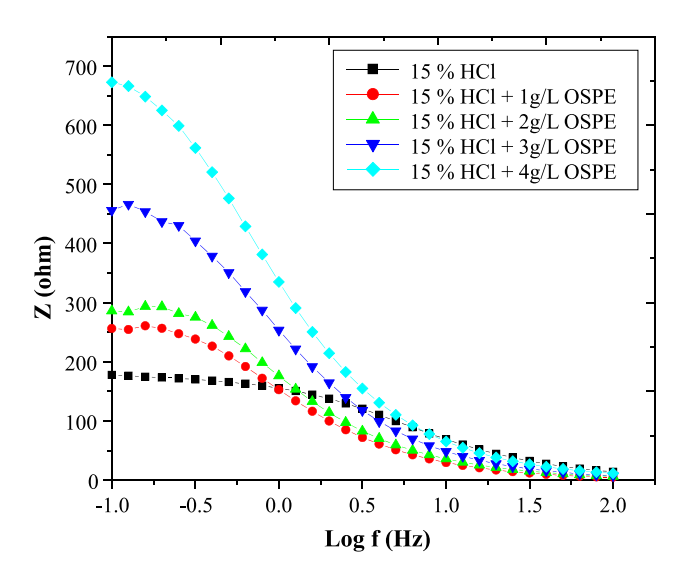


Figure 6: Bode-Z plots for SS-410 in 15% hydrochloric acid (HCl) without and with the different concentrations of Oryza sativa plant extract (OSPE) at 298 K.

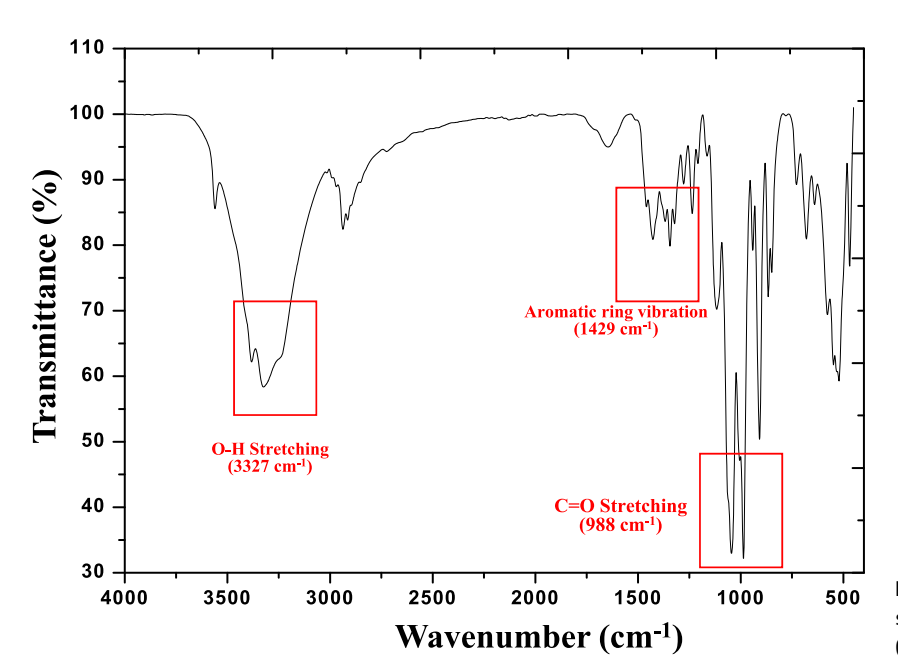
#### 3.5 UV-visible spectroscopic study

Figure 8 shows the UV-vis spectra of OSPE in 15% HCl solutions before and after immersion of the stainless steel sample SS-410. A higher UV-vis absorption intensity was observed for the OSPE solution before immersion of the stainless steel sample compared to the OSPE solution after immersion of SS-410 sample (after the corrosion test). In both cases, peaks representing the  $\pi-\pi^*$  and  $n-\pi^*$  transitions are observed at 214 nm and 360 nm, respectively. The intensity of the visible UV peak of OSPE in 15% HCl solution after the stainless steel sample was immersed, was lower compared to the sample before immersion of SS-410. This decrease in peak intensity clearly shows the adsorption of OSPE components on the SS-410 surface, causing the free (not adsorbed) components to decrease, resulting in a decrease in peak intensity [28, 29].

#### 3.6 Surface investigation

#### 3.6.1 Scanning electron microscopy

The surface morphology of SS-410 in 15% HCl solution was analyzed by SEM. Figure 9 shows SEM images of (A) an abraded SS-410 sample, (B) an SS-410 sample immersed in 15% HCl solution without OSPE, and (C) an SS-410 sample



**Figure 7:** Fourier Transform Infra-Red (FTIR) spectrum of the *Oryza sativa* plant extract (OSPE).

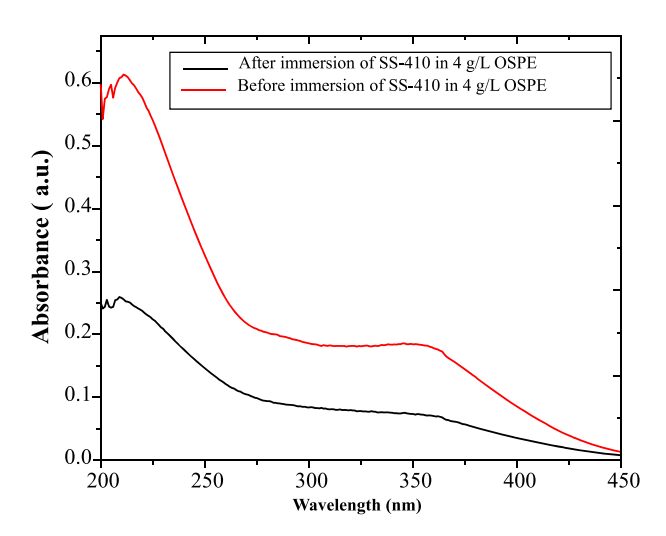


Figure 8: UV-vis spectra of the *Oryza sativa* plant extract (OSPE) after and before immersion of SS-410 for 24 h at 298 K.

immersed in 15% HCl solution with 4 g/L OSPE. From the SEM analysis, the SS-410 sample immersed in 15% HCl solution shows a rough and corroded surface, while the surface of the SS-410 sample immersed in OSPE with 15% HCl solution appears smooth due to the corrosion-inhibiting effect of OSPE [30, 31].

#### 3.6.2 Atomic force microscopy

Figure 9 shows the images of (A) the abraded SS-410 sample, (B) the SS-410 sample immersed in the 15% HCl

solution without OSPE, and (C) the SS-410 sample immersed in the 15% HCl solution with 4 g/L OSPE solution obtained by AFM. The value of surface roughness for the abraded SS-410 sample and the SS-410 sample immersed in 15% HCl solution are 26.83 nm and 939.14 nm, respectively. The significant increase in surface roughness after immersion in the HCl solution without OSPE indicates the degree of corrosion, as the surface of the abraded SS-410 samples loses smoothness due to corrosion [32, 33]. The SS-410 sample immersed in HCl with 4 g L $^{-1}$  OSPE had a comparatively lower surface roughness of 311.67 nm, which can be attributed to the corrosion-inhibiting effect of the phytochemicals contained in the OSPE.

#### 3.6.3 X-ray diffraction (XRD) study

XRD spectra were obtained for SS-410, SS-410 immersed in 15% HCl and SS-410 immersed in 15% HCl with 4 g/L OSPE. It can be seen from Figure 10 that the intensity of the iron peak at (40–50)° is weak in the case of the SS-410 sample immersed in 15% HCl compared to the unexposed SS-410 sample and the SS-410 sample immersed in HCl with OSPE. The presence of iron oxide peaks at (20–30)° in the SS-410 sample immersed in 15% HCl without OSPE also confirmed the formation of iron oxide as a result of corrosion. These peaks were absent in the unexposed SS-410 sample and in the SS-410 sample immersed in 15% HCl with 4 g/L OSPE. The XRD study confirms the protective effect of OSPE against corrosive media on the surface of SS-410 [34].

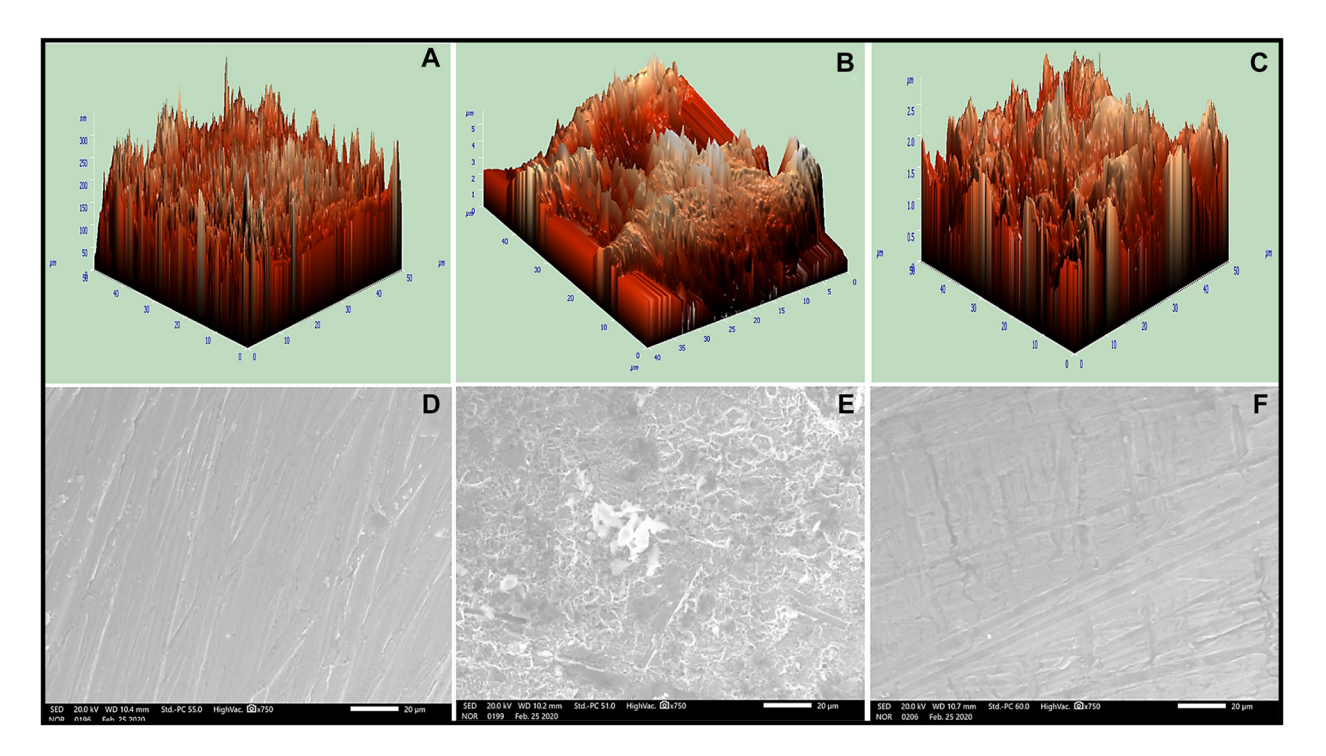


Figure 9: (A, D) Images of scanning electron microscopy (SEM), atomic force microscopy (AFM) for abraded SS-410, (B, E) images of SEM, AFM for SS-410 immersed in 15% hydrochloric acid (HCl) solution, (C, F) images of SEM, AFM for SS-410 immersed in 15% HCl solution with 4 g/L *Oryza sativa* plant extract (OSPE).

#### 3.7 Theoretical studies

#### 3.7.1 Frontier molecular orbitals and their parameters

The frontier molecular orbital density distributions (LUMO and HOMO) of the optimum structures of phytochemicals

presents in OSPE are shown in Figure 11. The key parameters of quantum chemical calculations are: energy of the highest occupied molecular orbital ( $E_{\rm HOMO}$ ), energy of the lowest unoccupied molecular orbital ( $E_{\rm LUMO}$ ), the energy gap between LUMO and HOMO ( $\Delta E$ ), the back donation energy ( $\Delta E_{\rm Back\,donation}$ ), the global hardness ( $\sigma$ ), and the softness ( $\eta$ )

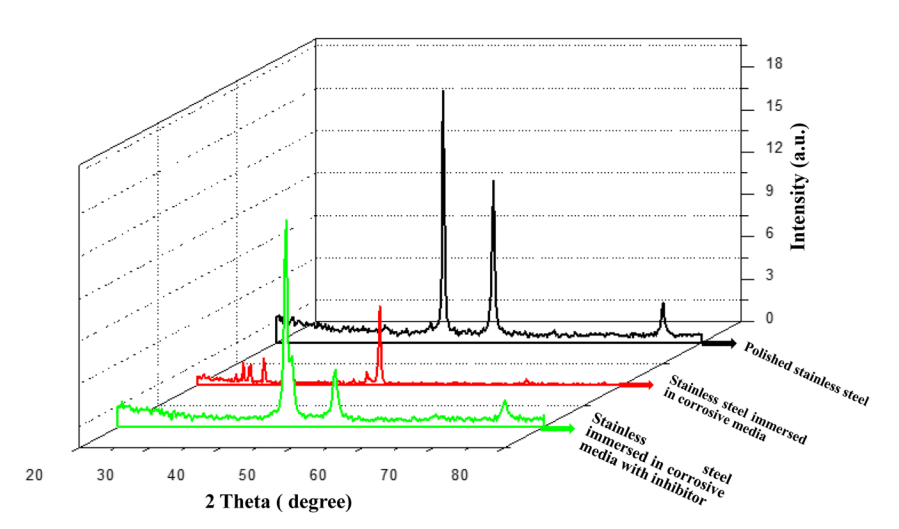


**Figure 10:** XRD spectra on the surface of stainless steel SS-410.

[35–38]. These parameters were calculated using Equations (12)-(15):

$$\Delta E = E_{\text{LUMO}} - E_{\text{HOMO}} \tag{12}$$

$$\eta = \frac{1}{2} \left( E_{\text{LUMO}} - E_{\text{HOMO}} \right) \tag{13}$$

$$\sigma = \frac{1}{\eta} \tag{14}$$

$$\sigma = \frac{1}{\eta}$$
 (14)  
$$\Delta E_{\text{Back donation}} = -\frac{\eta}{4}$$
 (15)

The change in the parameters of the theoretical study make clear how the phytochemicals contained in the OSPE interacted with the SS-410 surface (see Table 4). The energy of highest occupied molecular orbital follows the order: 9,12,15-octadecatrienoic acid-2,3-dihydroxypropyl ester > tetradecanoic acid > 28-homotyphasterol which indicated the order of donation of electrons to the vacant orbital of iron. 9,12,15-octadecatrienoic acid-2,3-dihydroxypropyl ester has the lowest  $\Delta E$  (1.339 eV), demonstrating the good stability of the [9,12,15-octadecatrienoic acid2,3-dihydroxypropyl ester-Fel complex. The higher value of  $\Delta E$ -back donation of 9,12,15-octadecatrienoic acid-2,3-dihydroxypropyl ester compared to the other two compounds shows the higher stability of the [Fe-9,12,15-octadecatrienoic acid-2,3-dihydroxypropyl ester complex. Hence, the inhibition effect follows the order 9,12,15-octadecatrienoic acid-2,3-dihydroxypropyl ester > tetradecanoic acid > 28-homotyphasterol. Therefore, 9,12,15-octadecatrienoic acid-2,3-dihydroxypropyl ester can be assumed to be the most essential component in the inhibition performance of the OSPE.

#### 3.7.2 Mulliken charge distribution

Mulliken charges have long been employed to investigate the adsorption active sites and the donor-acceptor electron interaction between inhibitor and iron atoms [3, 4, 39, 40]. In the gas phase, the optimal shape and Mulliken charges of neutral and protonated inhibitor atoms were studied. Table 5 represented the C and O atomic charges derived via

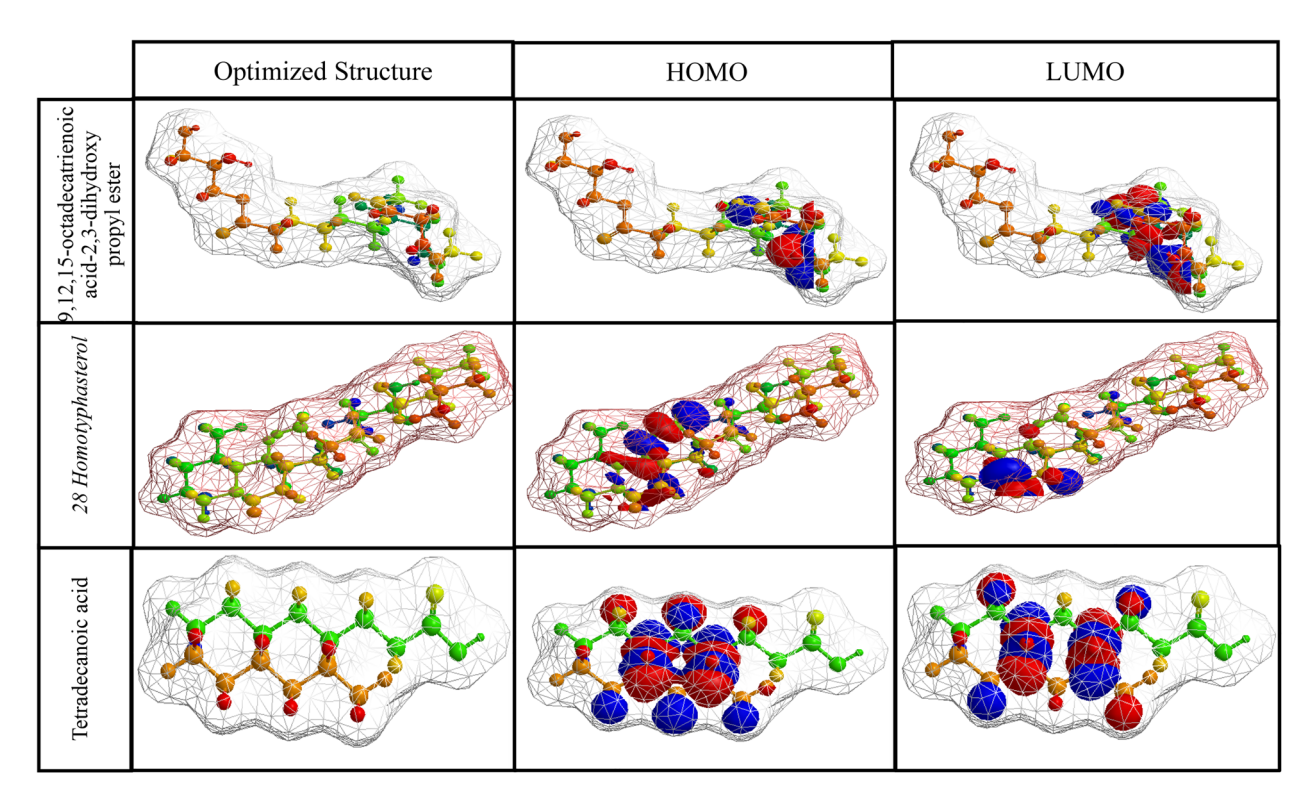


Figure 11: Optimized structures and frontier molecular orbital density distributions (HOMO and LUMO) obtained by the DFT/B3LYP/6-31G+(d,p) method of phytochemicals present in OSPE.

Table 4: Calculated quantum chemical parameters of phytochemicals of Oryza sativa plant extract (OSPE) analog obtained from the DFT/ B3LYP/6-31G+(d,p) method in the gas phase.

S. no	Phytochemicals	E <sub>HOMO</sub> /eV	E <sub>LUMO</sub> /eV	Δ <i>E</i> /eV	η/eV	$\sigma/{ m eV}^{-1}$	$\Delta E_{\mathrm{B.D/eV}}$
1	tetradecanoic acid	18.960	20.629	1.669	0.834	1.199	-0.417
2	9,12,15-octadecatrienoic acid-2,3-dihydroxypropyl ester	1.226	2.719	1.493	0.746	1.339	-0.186
3	28-homotyphasterol	-6.487	-1.234	5.253	2.626	0.380	-0.656

Mulliken charges in this study. The major active atoms that could form coordinating bonds due to the lone electron pairs and empty d-orbital of iron atoms were: 09 and O20 for tetradecanoic acid, O1, O5, O8, and O37 for 9,12,15-octadecatrienoic acid-2,3-dihydroxypropyl ester, and O19, O27, and O36 for 28-homotyphasterol. In addition, some carbon atoms in protonated inhibitors have a significant negative charge, which might function as active sites.

Table 5: Mullikin charges of atoms present in phytochemicals.

Tetradecanoic acid						
Atom	Mullikin charge	Atom	Mullikin charge	Atom	Mullikin charge	
C1	-0.065	C7	0.260	C15	0.704	
C2	-0.044	09	-0.431	C16	-0.301	
C3	0.0895	C11	-0.065	020	-1.105	
C4	-0.037	C12	0.044			
C5	0.069	C13	0.008			
C6	-0.041-	C14	-0.040			
9,12,15-0	ctadecatrien	oic acid	l-2,3-dihydroxyp	ropyl e	ster	
01	-0.387	C11	-0.110	C20	-0.096	
C2	0.199	C13	-0.079	C21	-0.864	
C3	0.146	C14	0.008	C22	-0.887	
C4	0.200	C15	0.410	C23	-0.100	
05	-0.396	C16	1.142	C24	-0.482	
C7	0.152	C17	-0.133	C25	-0.192	
08	-0.403	C18	0.295	C26	-0.145	
C10	-0.589	C19	-0.440	037	-1.05	
28-homot	typhasterol					
C1	-0.011	C12	-0.081	C24	0.017	
C2	-0.077	C13	-0.122	C25	-0.292	
C3	0.220	C14	-0.093	C26	-0.146	
C4	-0.080	C15	-0.081	027	-0.99	
C5	-0.010	C16	-0.078	029	-0.399	
C6	0.024	C17	-0.027	C31	-0.010	
C7	0.419	019	-0.578	C32	-0.145	
C8	-0.064	C20	-0.009	C33	-0.038	
C9	-0.016	C21	0.203	C35	0.287	
C10	-0.155	C22	0.153	036	0.399	
C11	-0.003	C23	-0.014			

#### 3.7.3 Proposed mechanism of adsorption

The mechanism of corrosion inhibition of SS-410 by OSPE in 15% HCl solution can be explained on the basis of molecular adsorption. There are two possible mechanisms: i) the donor-acceptor interactions between the  $\pi$ -electrons of OSPE and the empty *d*-orbitals of the SS-410 surface; ii) the interaction between the electrons of the heteroatoms in the inhibitor and the empty d-orbital of iron in SS-410, as shown in Figure 12. Many researchers have investigated plant extracts for their corrosion inhibitory potential in acidic media, especially in HCl, at different extract concentrations. In these studies, higher concentrations of plant extracts were also used in less acidic media. In the present study, the corrosion inhibitory properties of OSPE in 15% HCl solution were investigated to address the problem of petroleum industry in real time. Since plant wastes are used as inhibitor source, the use of OSPE in higher concentration would not affect the environment. The comparative analysis of some of the reported plant

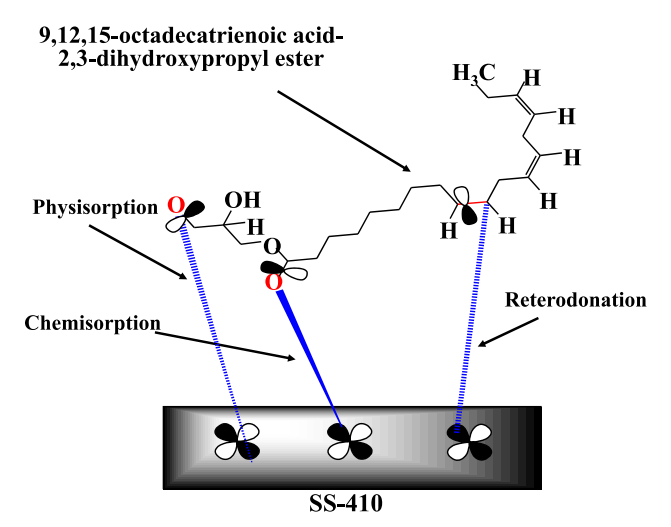


Figure 12: Schematic representation of the adsorption behavior of the key phytochemical, 9,12,15-octadecatrienoic acid-2,3-dihydroxypropyl ester molecule on the surface of SS-410.

Table 6: Comparative analysis of some reported plant-based corrosion inhibitors in different corrosive media.

Plant name	Concentration/g L <sup>-1</sup>	Corrosive media	Inhibition efficiency/%	Reference
Oryza sativa	4.0	15% HCl	91.92	Present study
Marrubium vulgare L.	8.0	1 M HCl	86.51	[40]
Tender arecanut	4.5	0.5 M HCl	95.50	[41]
Polyaspartic acid	10	5 M H <sub>2</sub> SO <sub>4</sub>	80.33	[42]
Pectin	8	2 M HCl	94.40	[43]
Matricaria recutita	7.2	1 M HCl	93.28	[44]
Opuntia ficus indica	5.0	1 M HCl	91.76	[45]
Malus domestica	5.0	0.5 M HCl	87.9	[46]
Ocimum basilicum L.	5.7	0.5 M HCl	90.10	[47]
Citrus sinensis	4.0	5 M HCl	93.38	[48]
Barley agriculture waste	5.0	1 M HCl	97.10	[49]
Phyllanthus muellerianus	6.7	3.5% NaCl	97.58	[50]
Verbena	6.0	1 M HCl	81.10	[51]
Thymus vulgaris	10.0	$5 \text{ M H}_2 \text{SO}_4$	88.60	[52]
Xylopia aethiopica	10.0	5 M H <sub>2</sub> SO <sub>4</sub>	47.80	[52]
Zingiber officinale	10.0	$5 \text{ M H}_2 \text{SO}_4$	79.60	[52]

inhibitors with the plant we studied, O. stavia, is shown in Table 6 [40-52].

Research funding: None declared.

Conflict of interest statement: The authors declare no conflicts of interest regarding this article.

#### 4 Conclusions

OSPE was investigated as a corrosion inhibitor for SS-410 stainless steel. Various techniques confirmed the corrosioninhibiting effect of OSPE. Gravimetric analysis showed a maximum of 91.92% at a concentration of 4 g/L OSPE in 15% HCl solution. PDP analysis showed that OSPE exerted mixed corrosion inhibition. SEM and AFM studies confirmed a remarkable change in the morphology of the SS-410 surface when exposed to a corrosive solution; the presence of OSPE attenuated the corrosive effect of the HCl solution. The mechanism of corrosion inhibition is based on adsorption. The adsorption of the inhibitor molecules was best fitted with the Langmuir adsorption isotherm. The theoretical quantum chemical calculations also supported the corrosion inhibition due to adsorption of inhibitor molecules from the OSPE. The parameters studied also showed that the 9,12,15-octadecatrienoic acid 2,3-dihydroxypropyl ester present in the OSPE was mainly responsible for the corrosion inhibitory performance.

Acknowledgment: Authors are thankful to Lovely Professional University for the support and the provision of the central instrumental facility.

Author contributions: All the authors have accepted responsibility for the entire content of this submitted manuscript and approved submission.

#### References

- 1. Koch G. Cost of corrosion, In Woodhead Publishing Series in Energy, Trends in Oil and Gas Corrosion Research and Technologies; El-Sherik A. M., Ed. Woodhead Publishing: Cambridge, Massachusetts, 2017; pp. 3-30, ISBN 978008101105.
- 2. Liu G. Q., Zhu Z. Y., Ke W., Han E. H., Zeng C. L. "Corrosion behavior of stainless steels and nickel-based alloys in acetic acid solutions containing bromide ions." Corrosion 2001, 57, 730-738; https://doi.org/10.5006/1.3290401.
- 3. Zhang W., Li H. J., Chen L., Sun J., Ma X., Li Y., Wu Y. C. Performance and mechanism of a composite scaling-corrosion inhibitor used in seawater: 10-Methylacridinium iodide and sodium citrate. Desalination 2020, 486, 114482; https://doi.org/ 10.1016/j.desal.2020.114482.
- 4. Zhang W., Ma R., Liu H., Liu Y., Li S., Niu L. Electrochemical and surface analysis studies of 2-(quinolin-2-yl) quinazolin-4 (3H)one as corrosion inhibitor for Q235 steel in hydrochloric acid. J. Mol. Liq. 2016, 222, 671–679; https://doi.org/10.1016/j.molliq. 2016.07.119.
- 5. Zhang W., Wang Y., Li H. J., Liu Y., Tao R., Guan S., Wu Y. C. Synergistic inhibition effect of 9-(4-chlorophenyl)-1, 2, 3, 4-tetrahydroacridines and Tween-80 for mild steel corrosion in acid medium. J. Phys. Chem. C 2019, 123, 14480-14489; https://doi.org/10.1021/acs.jpcc.9b02595.
- 6. Zhang W., Li H. J., Wang M., Wang L. J., Zhang A. H., Wu Y. C. Highly effective inhibition of mild steel corrosion in HCl solution by using pyrido [1, 2-a] benzimidazoles. New J. Chem. 2019, 43, 413-426; https://doi.org/10.1039/C8NJ04028A.

- 7. Zhang W., Liu Y., Zhang Y., Wang L. J., Wu Y. C., Li H. J. 9-Substituted acridines as effective corrosion inhibitors for mild steel: electrochemical, surface morphology, and computational studies. New J. Chem. 2020, 44, 6464-6474; https://doi.org/10. 1039/D0NJ00440E.
- 8. Nik W. W., Hajar H. M., Suriani M. J., Sabri M. G. M., Ghazali M. J. Development of anti-corrosive paint incorporated with henna extract as a natural inhibitor. J. Mech. Eng. Sci. 2017, 11, 3179-3188; https://doi.org/10.15282/jmes.11.4.2017.20.0286.
- 9. Nik W. W., Zulkifli F., Sulaiman O., Samo K. B., Rosliza R. September. Study of Henna (Lawsonia inermis) as natural corrosion inhibitor for aluminum alloy in seawater. In IOP Conference Series: Materials Science and Engineering, IOP Publishing: England and Wales, Vol. 36, 2012; p. 012043.
- 10. Bhardwaj N., Sharma P., Kumar V. Phytochemicals as steel corrosion inhibitor: an insight into mechanism. Corrosion Rev. 2021, 33, 1389-1395; https://doi.org/10.1515/corrrev-2020-0046.
- 11. Bhardwaj N., Sharma P., Kumar V. Anti-corrosive behaviour of Saccharum officinarum extract in 15 % HCl for stainless steel-410 surface. Asian J. Chem. 2021, 39, 27-41; https://doi.org/10. 14233/ajchem.2021.23194.
- 12. Mobin M., Noori S. Adsorption and corrosion inhibition behaviour of zwitterionic gemini surfactant for mild steel in 0.5 M HCl. Tenside Surfactants Deterg. 2016, 53, 357-367; https://doi.org/ 10.3139/113.110442.
- 13. Hellsten M., Karlsson G., Emanuelsson J. Alkyl phosphates as inhibitors for metal corrosion in detergents containing chelating agents. Tenside Surfactants Deterg. 1971, 8, 237-247; https://doi.org/10.1515/tsd-1972-090402.
- 14. Hameed R. A. Schiff'bases as corrosion inhibitor for aluminum alloy in hydrochloric acid medium. Tenside Surfactants Deterg. 2019, 56, 209-215; https://doi.org/10.3139/113.110622.
- 15. Liu G. Evaluation of polyether copolymer as green scale and corrosion inhibitor in seawater. Tenside Surfactants Deterg. 2019, 56, 197-208; https://doi.org/10.3139/113.110620.
- 16. Ghiaty E. A., Mohamed D. E., Badr E. A., Gad E. A., Soliman E. A., Aiad I. A. Experimental and computational study of ecofriendly synthesize d imine cationic surfactants as corrosion inhibitors for carbon steel in 1 M HCl. Tenside Surfactants Deterg. 2020, 57, 45-56; https://doi.org/10.3139/113.110659.
- 17. Meng B., Feng X., Qiu G., Liang P., Li P., Chen C., Shang L. The process of methylmercury accumulation in rice (Oryza sativa L.). Environ. Sci. Technol. 2011, 45, 2711-2717; https://doi.org/10. 1007/s10886-011-9991.
- 18. El Bribri A., Tabyaoui M., Tabyaoui B., El Attari H., Bentiss F. The use of Euphorbia falcata extract as eco-friendly corrosion inhibitor of carbon steel in hydrochloric acid solution. Mater. Chem. Phys. 2013, 141, 240-247; https://doi.org/10.1016/j. matchemphys.2013.05.006.
- 19. Odewunmi N. A., Umoren S. A., Gasem Z. M. Utilization of watermelon rind extract as a green corrosion inhibitor for mild steel in acidic media. J. Ind. Eng. Chem. 2015, 21, 239-247; https://doi.org/10.1016/j.jiec.2014.02.030.
- 20. Saady A., Rais Z., Benhiba F., Salim R., Alaoui K. I., Arrousse N., Zarrouk A. Chemical, electrochemical, quantum, and surface analysis evaluation on the inhibition performance of novel imidazo [4, 5-b] pyridine derivatives against mild steel corrosion.

- Corrosion Sci. 2021, 189, 109621; https://doi.org/10.1016/j. corsci.2021.109621.
- 21. Soltani N., Tavakkoli N., Kashani M. K., Mosavizadeh A. E. E. O., Oguzie E. E., Jalali M. R. Silybum marianum extract as a natural source inhibitor for 304 stainless steel corrosion in 1.0 M HCl. J. Ind. Eng. Chem. 2014, 20, 3217-3227; https://doi.org/10.1016/ i.jiec.2013.12.002.
- 22. Zulkifli F., Yusof M. S. M., Isa M. I. N., Yabuki A., Nik W. W. Henna leaves extract as a corrosion inhibitor in acrylic resin coating. Prog. Org. Coating 2017, 10, 310-319; https://doi.org/10.1016/j. porgcoat.2017.01.017.
- 23. Srivastava M., Tiwari P., Srivastava S. K., Prakash R., Ji G. Electrochemical investigation of Irbesartan drug molecules as an inhibitor of mild steel corrosion in 1 M HCl and 0.5 M H2SO4 solutions. J. Mol. Liq. 2017, 236, 184-197; https://doi.org/10. 1016/j.molliq.2017.04.017.
- 24. Hashim N. Z. N., Kassim K., Zaki H. M., Alharthi A. I., Embong Z. XPS and DFT investigations of corrosion inhibition of substituted benzylidene Schiff bases on mild steel in hydrochloric acid. Appl. Surf. Sci. 2019, 476, 861-877; https://doi.org/10.1016/j.apsusc. 2019.01.149.
- 25. Aksüt A. A., Lorenz W. J., Mansfeld F. The determination of corrosion rates by electrochemical dc and ac methods-II. Systems with discontinuous steady state polarization behavior. Corrosion Sci. 1982, 22, 611–619; https://doi.org/10.1016/0010-938X(81) 90015-9.
- 26. Idouhli R., Koumya Y., Khadiri M., Aityoub A., Abouelfida A., Benyaich A. Inhibitory effect of Senecio anteuphorbium as green corrosion inhibitor for \$300 steel. Int. J. Integrated Care 2019, 10, 133-143; https://doi.org/10.1007/s40090-019-0179-2.
- 27. Lorenz W. J., Mansfeld F. Determination of corrosion rates by electrochemical DC and AC methods. Corrosion Sci. 1981, 21, 647-672; https://doi.org/10.1016/0010-938X(81)90015-9.
- 28. Alaneme K. K., Olusegun S. J., Adelowo O. T. Corrosion inhibition and adsorption mechanism studies of Hunteria umbellata seed husk extracts on mild steel immersed in acidic solutions. Alexandria Eng. J. 2016, 55, 673-681; https://doi.org/10.1016/j. aej.2015.10.009.
- 29. Ogunleye O. O., Arinkoola A. O., Eletta O. A., Agbede O. O., Osho Y. A., Morakinyo A. F., Hamed J. O. Green corrosion inhibition and adsorption characteristics of Luffa cylindrica leaf extract on mild steel in hydrochloric acid environment. Heliyon 2020, 6, 3205; https://doi.org/10.1016/j.heliyon.2020.e03205.
- 30. Ramakrishnan P. J., Janardhanan V. D. K., Sreekumar R., Mohan K. P. Investigation on the effect of green inhibitors for corrosion protection of mild steel in 1 M NaOH solution. Int. J. Corrosion 2014, 2014, 487103; https://doi.org/10.1155/2014/ 487103.
- 31. Leena P., Zeinul Hukuman N. H., Biju A. R., Jisha M. Studies on methanolic extract of Lepidagathis keralensis as green corrosion inhibitor for mild steel in 1M HCl. J. Electrochem. Sci. Technol. 2019, 10, 231-243; https://doi.org/10.5229/JECST.2019.10.2.
- 32. Talib N. A. A., Zakaria S., Hua C. C., Othman N. K. Tannin bark Melalauca cajuputi powell (gelam) as green corrosion inhibitor of mild steel. In AIP Conference Proceedings, AIP, College Park: Maryland, Vol. 1614, 2014; pp. 171-177. https://doi.org/10.1063/ 1.4895191.

- 33. Yaocheng Y., Caihong Y., Singh A., Lin Y. Electrochemical study of commercial and synthesized green corrosion inhibitors for N80 steel in acidic liquid. New J. Chem. 2019, 43, 16058-16070; https://doi.org/10.1039/C9NJ03378E.
- 34. Gupta N. K., Joshi P. G., Srivastava V., Quraishi M. A. Chitosan: a macromolecule as green corrosion inhibitor for mild steel in sulfamic acid useful for sugar industry. Int. J. Biol. Macromol. 2018, 106, 704-711; https://doi.org/10.1016/j.ijbiomac.2017. 08 064
- 35. Verma C., Quraishi M. A., Ebenso E. E., Bahadur I. A green and sustainable approach for mild steel acidic corrosion inhibition using leaves extract: experimental and DFT studies. J. Bio-and Tribo-Corrosion 2018, 4, 1-12; https://doi.org/10.1007/s40735-018-0150-3.
- 36. Deng S., Li X. Inhibition by Ginkgo leaves extract of the corrosion of steel in HCl and H2SO4 solutions. Corrosion Sci. 2012, 55, 407-415; https://doi.org/10.1016/j.corsci.2011.11.005.
- 37. Hassan K. H., Khadom A. A., Kurshed N. H. Citrus aurantium leaves extracts as a sustainable corrosion inhibitor of mild steel in sulfuric acid. S. Afr. J. Chem. Eng. 2016, 22, 1-5; https://doi. org/10.1016/j.sajce.2016.07.002.
- 38. Al-Azawi K. F., Mohammed I. M., Al-Baghdadi S. B., Salman T. A., Issa H. A., Al-Amiery A. A., Gaaz T. S., Kadhum A. A. H. Experimental and quantum chemical simulations on the corrosion inhibition of mild steel by 3-((5-(3, 5-dinitrophenyl)-1, 3, 4-thiadiazol-2-yl) imino) indolin-2-one. Results Phys. 2018, 9, 278-283; https://doi.org/10.1016/j.rinp.2018.02.055.
- 39. Zhang W., Li H. J., Wang M., Wang L. J., Shang F., Wu Y. C. Halogensubstituted acridines as highly effective corrosion inhibitors for mild steel in acid medium. J. Phys. Chem. C 2018, 122, 25349-25364; https://doi.org/10.1021/acs.jpcc.8b07015.
- 40. Hmamou D. B., Salghi R., Zarrouk A., Zarrok H., Benali O., Errami M., Hammouti B. Inhibition effect of horehound (Marrubium vulgare L.) extract towards C38 steel corrosion in HCl solution. Res. Chem. Intermed. 2013, 39, 3291-3302; https://doi. org/10.1007/s11164-012-0840-2.
- 41. Raghavendra N., Bhat J. I. Green approach to inhibition of corrosion of aluminum in 0.5 M HCl medium by tender arecanut seed extract: insight from gravimetric and electrochemical studies. Res. Chem. Intermed. 2016, 42, 6351-6372; https://doi. org/10.1007/s11164-016-2467-1.
- 42. Cui R., Gu N., Li C. Polyaspartic acid as a green corrosion inhibitor for carbon steel. Mater. Corros. 2011, 62, 362-369; https://doi. org/10.1002/maco.200905511.
- 43. Fares M. M., Maayta A. K., Al-Qudah M. M. Pectin as promising green corrosion inhibitor of aluminum in hydrochloric acid solution. Corrosion Sci. 2012, 60, 112-117; https://doi.org/10. 1016/j.corsci.2012.04.002.
- 44. Nasibi M., Zaarei D., Rashed G., Ghasemi E. Chamomile (Matricaria recutita) extract as a corrosion inhibitor for mild steel in hydrochloric acid solution. Chem. Eng. Commun. 2013, 200, 367-378; https://doi.org/10.1080/00986445.2012.709475.
- 45. Ghazi Z., ELmssellem H., Ramdani M., Chetouani A., Rmil R., Aouniti A., Hammouti B. Corrosion inhibition by naturally occurring substance containing Opuntia-Ficus Indica extract on the corrosion of steel in hydrochloric acid. J. Chem. Pharmaceut. Res. 2014, 6, 14171425.
- 46. Umoren S., Obot I. B., Gasem Z., Odewunmi N. A. Experimental and theoretical studies of red apple fruit extract as green corrosion inhibitor for mild steel in HCl solution. J. Dispersion Sci. Technol. 2015, 36, 789-802; https://doi.org/10.1080/01932691. 2014.922887.

- 47. Halambek J., Žutinić A., Berković K. Ocimum basilicum L. oil as corrosion inhibitor for aluminium in hydrochloric acid solution. Int. J. Electrochem. Sci. 2013, 8, 11201-11214.
- 48. Kumar H., Yadav V. Citrus sinensis peels as a green corrosion inhibitor for mild steel in 5.0 M hydrochloric acid solution. Res. J. Chem. Sci. 2016, 6, 53-60.
- 49. Matos L. A. C., Taborda M. C., Alves G. J. T., Cunha M. T., Banczek E. P., Oliveira M. F., Rodrigues P. R. P. Application of an acid extract of barley agro-industrial waste as a corrosion inhibitor for S.S.AISI 304 in H 2 SO 4. Int. J. Electrochem. Sci. 2018, 13, 1577-1593; https://doi.org/10.20964/2018.02.01.
- 50. Okeniyi J. O., Omotosho O. A., Ogunlana O. O., Okeniyi E. T., Owoeye T. F., Ogbiye A. S., Ogunlana E. O. Investigating prospects of Phyllanthus muellerianus as eco-friendly/ sustainable material for reducing concrete steel-reinforcement corrosion in industrial/microbial environment. Energy Procedia 2015, 74, 1274-1281; https://doi.org/10.1016/j.egypro.2015.07. 772.
- 51. Hmamou D. B., Salghi R., Zarrouk A., Al-Deyab S. S., Zarrok H., Hammouti B., Errami E. Verbena extract: an efficient inhibitor of C38 steel corrosion in hydrochloric acid. Int. J. Electrochem. Sci. 2012, 7, 6234-6246.
- 52. Okafor P. C., Apebende E. A. Corrosion inhibition characteristics of Thymus vulgaris, Xylopia aethiopica and Zingiber officinale extracts on mild steel in H2SO4 solutions. Pigment Resin Technol. 2014, 42, 6351-6372; https://doi.org/10.1108/PRT-07-2013-0060.

#### **Bionotes**

#### Nishant Bhardwai

Nishant Bhardwaj received his M.Sc. degree in Industrial Chemistry from Punjab University, India in 2016 and his B.Sc. degree in Industrial Chemistry from Kurukshetra University, India. He is currently pursuing his Ph. D in Organic Chemistry, under the supervision of Dr. Vineet Kumar, School of Biosciences and Bioengineering, Lovely Professional University, India. His research area mainly focuses on the development of effective green corrosion inhibitors for metal protection for industrial applications.

#### Pooja Sharma

Pooja Sharma received her M.Sc. degree in Biotechnology from DAV University, India in 2017 and her B.Sc. degree in Medical Lab Technology from Punjab Technical University, India. She is currently pursuing her Ph. D in Biotechnology under the supervision of Dr. Vineet Kumar, School of Biosciences and Bioengineering, Lovely Professional University, India. Her research focuses on synthesis of green nanomaterials and their applications in biomedical corrosion and also the development of nanomaterials for theranostic applications.

Vineet Kumar is currently working as Assistant Professor at the Department of Biotechnology, LPU, Jalandhar, India. Previously he was UGC-DSK postdoctoral fellow (2013-2016) at Panjab University, Chandigarh, India. His areas of interest include natural plant products, green synthesis of nanoparticles, nanotoxicity testing and application of nanoparticles. He has published many articles and books in these areas. He is also serving as editorial board member for various journals. https://orcid.org/0000-0002-8772-679X.